Phase matrix and cross sections for single scattering by circular cylinders: a comparison of ray optics and wave theory

Yoshihide Takano and Masayuki Tanaka

The phase matrix and several quantities for single scattering by an arbitrarily oriented circular cylinder are formulated by using the approximation of ray optics, which includes geometrical reflection and refraction plus Fraunhofer diffraction; then the effects of polarization are considered. Computations were made using electromagnetic wave theory and ray optics approximations for $m = 1.31\text{–}0.0i$ and $1.31\text{–}0.1i$. Results by these methods approach one another as the ratio of the cylinder's circumference to the incident wavelength increases. One of two ray optics approximations proposed requires less computation time than wave theory. The applicability of the ray optics approximation is dependent on the orientation of the cylinder relative to the incident light as well as the size parameter and, moreover, dependent on what quantity for single scattering is compared.

I. Introduction

The average length of ice crystals in cirriform clouds is several hundred micrometers[1,2] and considerably larger than the wavelength of radiation in the visible and near-IR regions, so that the ray optics approximation seems to be suitable. In order to obtain information on the light scattering properties of columnar ice crystals of hexagonal cylindrical shape, we shall consider in this study the light scattering by infinitely long homogeneous isotropic cylinders. The solution of scattering of electromagnetic plane waves by an infinitely circular cylinder was derived by Rayleigh[3] at normal incidence and by Wait[4] at oblique incidence. Since then numerous calculations have been performed by many investigators.[5–9] Recently the method of integral equations was applied to a hollow hexagonal cylinder.[10] To determine the diameter and the refractive index of a fiber, some approximate computations of backscattered light intensities from a circular cylinder have been performed by means of geometrical optics.[11,12] Similar computations of backscattered light intensities have been done by Holoubek[13] and Saekeang and Chu[14] in a more elaborate fashion. But a ray optics formulation including effects of polarization for light scattering by an arbitrarily oriented cylinder has not yet been performed. We shall develop the formulas of light scattering by a cylinder on the basis of the ray optics approximation[5] and compare computation results by this approximation with those by the exact solution of wave theory. The purpose of this comparison is to verify applicability of the ray optics approximation and to find the range of validity.

II. Scattering Geometry

Scattering geometry is shown in Fig. 1. In this study, we follow the geometry and notation by Liou.[7] The Z axis of the cylindrical coordinate system (r,ϕ,Z) is placed along the cylinder axis so that the cylinder occupies the region $r \leq a$, where a is the radius. The X axis is in the plane containing the direction of the incident light and the Z axis. The complement of the angle between the incident direction and the Z axis is denoted as an oblique incident angle α. The angle between the normal of the cylinder at the incident point, i.e., the radial direction of the cylinder and the negative X axis, is specified as β. Usually, we have only to consider rays with $0 \leq \beta \leq \pi/2$. Scattered radiation emerges along the surface of the cone with an apical angle $\pi - 2\alpha$, so that it can be expressed by ϕ denoted as an observation angle. We consider two polarization states of light, where electric vector $\mathbf{E}$ vibrates parallel to the plane containing the direction of propagation of light and the Z axis [case (l)] and the electric vector vibrates perpendicular to this plane [case (r)].

The authors are with Tohoku University, Faculty of Science, Upper Atmosphere Research Laboratory, Aoba Aramaki, Sendai 980, Japan.

Received 23 February 1980.
0003-6935/80/162781-13$00.50/0.

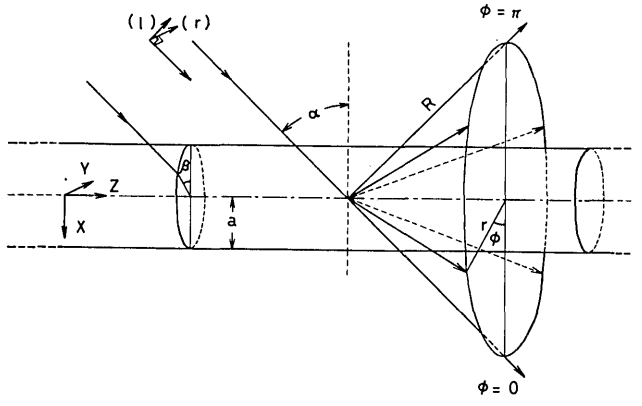

Fig. 1. Geometry for light scattered by an infinitely long circular cylinder. All symbols are explained in the text.

III. Ray Optics

We denote an amplitude matrix by **T** and a phase matrix by **G**, which transform the amplitude of electromagnetic fields and the Stokes parameters (I_l, I_r, U, V), respectively, of the incident light to those of the scattered light in a reference plane containing the direction of propagation of light and the Z axis. Amplitude matrix **T** thus defined is given by

$$\begin{pmatrix} E_{sl} \\ E_{sr} \end{pmatrix} = \left(\frac{2}{\pi kR\cos\alpha}\right)^{1/2} \exp[i(-kR + \omega t - 3\pi/4)] \begin{pmatrix} T_2 & T_3 \\ T_4 & T_1 \end{pmatrix} \begin{pmatrix} E_{il} \\ E_{ir} \end{pmatrix}, \quad (1)$$

where $\mathbf{E}_i$ and $\mathbf{E}_s$ are, respectively, the incident and scattered amplitudes of the electric vector, k is the wave number in vacuum, ω is the circular frequency, R is the distance from the apex of the cone, t is time, and $i = (-1)^{1/2}$. We alternatively define a matrix **A** as a multiple of **T**:

$$A_j(x,m,\alpha,\phi) = \left(\frac{2}{x\cos\alpha}\right)^{1/2} T_j(x,m,\alpha,\phi), \quad j = 1,2,3,4, \quad (2)$$

where x $(= 2\pi a/\lambda)$ denotes that the ratio of the circumference of the cylinder to the wavelength of incident light, m $(= m_r - im_i)$ is the complex index of refraction of the scattering medium. The matrix **A** is the amplitude matrix normalized by the square root of a multiple of the geometric shadow area $2a\cos\alpha$ per unit length of the cylinder, and its elements are expressed in the form

$$A_j(x,m,\alpha,\phi) = (\delta_{1j} + \delta_{2j})A_D + \sum_{p=0}^{N}\sum_{t=1}^{M_p} A_j^{(p)}[x,m,\alpha,\phi(\alpha,\beta_t)], \quad (3)$$

where δ_{kl} denotes the Kronecker delta, i.e., $\delta_{kl} = 1$ for $k = l$ and zero otherwise. A_D is the contribution from Fraunhofer diffraction that can be expressed from the scalar Kirchhoff approximation as

$$A_D(x,\alpha,\phi) = (2x\cos\alpha)^{1/2}\frac{\sin(x\cos\alpha\sin\phi)}{x\cos\alpha\sin\phi}. \quad (4)$$

The derivation of this formula is described in Appendix A. Since the factor $x\cos\alpha$ is included as a single parameter in Eq. (4), it is expected that the cylinder apparently shrinks as α becomes large. $A_j^{(p)}$ is the contribution from geometrical optics, which includes external reflection ($p = 0$), refraction ($p = 1$), and internal reflection of each order ($p \geq 2$): hereafter we call them the transmitted light of the pth order. The summation for t from 1 to M_p represents the contribution from rays with different incident points β_t and the same p. Clearly M_p is unity for $p = 0$ and for $p = 1$, but for $p \geq 2$, M_p can be more than 2 since $\phi(\alpha,\beta)$ is a multivalued function of β (Ref. 5, p. 229, and Ref. 13). The value N should theoretically be infinity, but in practice a small integer can be adopted with sufficient accuracy; $N = 4 \sim 9$ are sufficient to account for more than 99.9% of the scattered energy even for nonabsorbing cylinders except for cases with very large values of α. Amplitude matrix elements $A_j^{(p)}$ are given by

$$A_j^{(p)}[x,m,\alpha,\phi(\alpha,\beta_t)] = \epsilon_j^{(p)}\left(\frac{\pi\cos\beta}{|\partial\phi'/\partial\beta|}\right)^{1/2}\exp(i\gamma), \quad j = 1,2,3,4, \quad (5)$$

where

$$\epsilon^{(p)} = \begin{cases} \mathbf{L}_{-\delta 1}\mathbf{R}\mathbf{L}_{-\delta 1}, & \text{for } p = 0, \\ \mathbf{L}_{-\delta 1}\overline{\mathbf{T}}\,(\mathbf{L}_{\delta 2}\mathbf{C}\mathbf{R})^{p-1}\,\mathbf{L}_{\delta 2}\,\overline{\mathbf{T}}\mathbf{L}_{-\delta 1}, & \text{for } p \geq 1. \end{cases} \quad (6)$$

Matrix $\mathbf{L}_\delta$ denotes the rotation of the coordinate system:

$$\mathbf{L}_\delta = \begin{pmatrix} \cos\delta & \sin\delta \\ -\sin\delta & \cos\delta \end{pmatrix}, \quad (7)$$

R is the reflection matrix, and $\overline{\mathbf{T}}$ is the transmission matrix:

$$\mathbf{R} = \begin{pmatrix} r_\parallel & 0 \\ 0 & r_\perp \end{pmatrix}, \qquad \overline{\mathbf{T}} = \begin{pmatrix} (1-r_\parallel^2)^{1/2} & 0 \\ 0 & (1-r_\perp^2)^{1/2} \end{pmatrix} \quad (8)$$

where $r_\parallel$ and $r_\perp$ are the Fresnel reflection coefficients parallel and perpendicular, respectively, to the incident plane, i.e., the plane containing the directions of propagation of incident and reflected rays. The Fresnel reflection coefficients are given by

$$r_\parallel = \frac{m\cos\tau_i - \cos\tau_r}{m\cos\tau_i + \cos\tau_r}, \qquad r_\perp = \frac{\cos\tau_i - m\cos\tau_r}{\cos\tau_i + m\cos\tau_r}. \quad (9)$$

In the above equations, τ_i denotes the incident angle with reference to the normal,

$$\cos\tau_i = \cos\alpha\cos\beta, \quad (10)$$

and τ_r denotes the refracted angle given by Snell's law:

$$m\sin\tau_r = \sin\tau_i. \quad (11)$$

To determine the refracted direction, τ_r is approximated with the angle obtained by replacement of m with m_r in Eq. (11). In Eq. (6), matrix **C** is given by

$$\mathbf{C} = \begin{pmatrix} -1 & 0 \\ 0 & -1 \end{pmatrix}. \tag{12}$$

This matrix expresses a phase shift of π due to internal reflection. The relations $A_4^{(p)} = -A_3^{(p)}$ and therefore $A_4 = -A_3$ are valid from the property of $\epsilon_j^{(p)}$. Since the incident angle of any ray refracted once into the cylinder is always τ_r, the rotation angles of the coordinate system $\delta 1$ and $\delta 2$ are obtained from the spherical geometry shown in Figs. 2(a) and (b):

$$\sin\delta 1 = \sin\beta/\sin\tau_i, \tag{13}$$

$$\cos\delta 2 = -\cos^2\Delta + \sin^2\Delta\cos(2\xi), \tag{14}$$

where Δ and ξ are auxiliary angles:

$$\sin\Delta = \sin\alpha/\sin\tau_i, \tag{15}$$

$$\tan\xi = \cos\Delta\tan\tau_r. \tag{16}$$

From Fig. 2, it can also be understood that the scattered light is confined to the surface of a solid cone that forms an angle α with the X-Y plane. The factor $(\pi\cos\beta/|\partial\phi'/\partial\beta|)^{1/2}$ in Eq. (5) is derived from the conservation of the flux of radiant energy. Deviation angle ϕ' appearing in this factor is given by

$$\phi'(\alpha,\beta) = \pi - 2\beta - p(\pi - 2\xi). \tag{17}$$

This angle may express how many times and in what direction the ray rotates within the cylinder. The derivative $\partial\phi'/\partial\beta$ can be obtained straightforwardly from Eq. (17). The relation between deviation angle ϕ' and actual observation angle ϕ is

$$\phi'(\alpha,\beta) = 2\pi k + q\phi(\alpha,\beta), \tag{18}$$

where k is an integer, and q is $+1$ or -1. Namely, ϕ is the projection of ϕ' on the branch $[0,\pi]$ with a proper choice of k and q. The factor γ in Eq. (5) is a complex phase of a light ray except for that of the Fresnel coefficient already included in $\epsilon^{(p)}$:

$$\gamma = \frac{3}{4}\pi + \delta + \left[p + \frac{1}{2}(s-1)\right]\frac{1}{2}\pi, \tag{19}$$

where

$$\delta = 2x(\cos\tau_i - pm_r\cos\tau_r) + i\frac{2\pi m_i}{\lambda}pl, \tag{20}$$

$$l = \frac{2a\cos\tau_r}{1 - \sin^2\alpha/m_r^2}, \tag{21}$$

$$s = \operatorname{sgn}\left(-\frac{\partial\phi'}{\partial\beta}\right) = \frac{-\partial\phi'/\partial\beta}{|-\partial\phi'/\partial\beta|}. \tag{22}$$

The constant phase factor in Eq. (19) is taken to be $3\pi/4$, whereas this factor is $\pi/2$ in the case of a sphere (Ref. 5, p. 207). The real part of δ is the advance in phase of the actual ray due to the length of optical path with respect to a hypothetical ray scattered without phase lag at the apex of the cone. This term is exactly the same as the corresponding quantity for a sphere (Ref. 5, p. 207). The imaginary part of δ accounts for absorption within the cylinder, where pl is the total path length in the cylinder. The quantity $p + (s-1)/2$ in Eq. (19) is the number of focal lines through which the ray passes. With respect to the phase factor, it is proposed that the term $[-2k + (1-q)/2]\pi/2$, which appears in the case of a sphere (Ref. 5, p. 207), should not be included in the case of a cylinder because of the absence of the glory for nonspherical particles.

Now let us consider a cylinder at an oblique incident angle α, say, cylinder a, which scatters a light ray to an observation angle ϕ. Let us also take another cylinder, c, in the mirror image of cylinder a with respect to the scattering plane, which necessarily has the same oblique incident angle α and scatters a ray in the same direction in space as does cylinder a. The cylinder at the reciprocal position of cylinder a, say, cylinder b, and its mirror image, say, cylinder d, coincide with cylinders a and c, respectively. Taking these symmetry relations into consideration, the 4×4 phase matrix of these four cylinders, which transforms the Stokes parameters (I_l, I_r, U, V) from incident to scattered, is given, in van de Hulst's notation (Ref. 5, p. 44), by

$$\mathbf{G} = \begin{pmatrix} M_2 & \frac{1}{2}(M_3+M_4) & 0 & 0 \\ \frac{1}{2}(M_3+M_4) & M_1 & 0 & 0 \\ 0 & 0 & S_{12}+S_{34} & -D_{21} \\ 0 & 0 & D_{21} & S_{12}-S_{34} \end{pmatrix}, \tag{23}$$

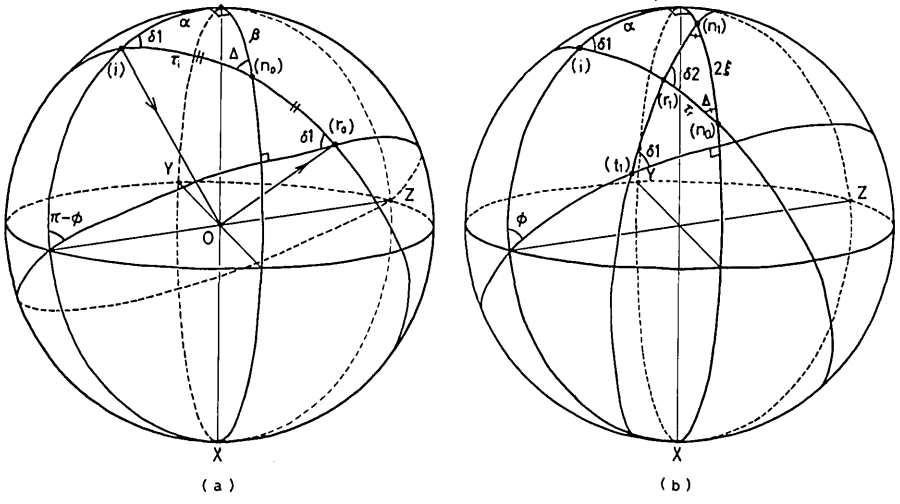

Fig. 2. (a) Spherical geometry of the externally reflected light. O denotes the incident point. (i), (n_0), and (r_0) express the incident ray, the normal, and the externally reflected ray, respectively. (b) Spherical geometry of the transmitted light of the first order. (r_1), (n_1), and (t_1) express the refracted ray, the normal, and the transmitted ray of the first order, respectively.

where we consider a direction for which scattering angle θ is neither zero nor π. From the relation $A_4 = -A_3$, we can easily find the relations $S_{34} = -M_3$ and $M_4 = M_3$. Then we have

$$\mathbf{G} = \begin{pmatrix} M_2 & M_3 & 0 & 0 \\ M_3 & M_1 & 0 & 0 \\ 0 & 0 & S_{12} - M_3 & -D_{21} \\ 0 & 0 & D_{21} & S_{12} + M_3 \end{pmatrix}. \tag{24}$$

In Eq. (24), five independent parameters occur for a polydispersion, and the relation

$$G_{44} - G_{33} = 2G_{12} \ (\geq 0) \tag{25}$$

is easily found. After ϕ' intersects $n\pi$ odd times (n = an integer), the ray with $-\pi/2 \leq \beta \leq 0$ contributes to the amplitude, so that the signs of $\delta 1$ and $\delta 2$ change. Therefore, whenever $\phi'(\alpha,\beta)$ takes the value of $n\pi$, $A_3^{(p)}$ and $A_4^{(p)}$ should be multiplied further by -1. In such a case, at $\phi = 0$ and $\phi = \pi$, there are two contributions to the amplitude coming from each side of a cylinder whose magnitudes are the same but with opposite signs, so that G_{12} should always be zero at these directions. On the other hand, G_{11} and G_{22} can have finite and small peaks at $\phi = 0$ or $\phi = \pi$ because there are two contributions to the amplitude from each side of a cylinder of the same magnitude and sign. A typical example is the case for $\alpha = 45°$ shown later.

For the incidence of unpolarized natural light with Stokes parameters (½,½,0,0), the phase function and the degree of linear polarization are given, respectively, by

$$G = \frac{1}{2}(G_{11} + G_{12} + G_{21} + G_{22}), \tag{26}$$

$$\mathrm{DP} = \frac{(G_{11} + G_{12}) - (G_{21} + G_{22})}{(G_{11} + G_{12}) + (G_{21} + G_{22})}. \tag{27}$$

If the phase matrix of randomly oriented cylinders is needed, the scattering plane should be taken as the reference plane. However, phase function G and element G_{44} are independent of the choice of the reference plane.

The scattering efficiency factor is defined by the total scattered energy integrated over all angles ϕ divided by the product of the incident intensity and the geometric shadow area per unit length. In the case of ray optics, with the definition of A_j in Eq. (2), this is given by

$$\begin{aligned} Q_{\mathrm{sca}} &= \frac{1}{2}(Q_{\mathrm{sca},l} + Q_{\mathrm{sca},r}) \\ &= \frac{1}{2}\left[\frac{1}{\pi}\int_0^{\pi}(G_{11} + G_{12})d\phi + \frac{1}{\pi}\int_0^{\pi}(G_{21} + G_{22})d\phi\right] \\ &= \frac{1}{\pi}\int_0^{\pi} G d\phi. \end{aligned} \tag{28}$$

And, accordingly, the scattering cross section per unit length of a cylinder is given as

$$C_{\mathrm{sca}} = 2a \cos\alpha Q_{\mathrm{sca}}. \tag{29}$$

The absorption efficiency factor Q_{abs} is the difference between the total energy impinging on the cylinder, which is assumed to be unity, and the externally reflected energy $E^{(0)}$ plus the transmitted energy $E^{(p)}$ ($p \geq 1$); i.e.,

$$\begin{aligned} Q_{\mathrm{abs}}(x,m,\alpha) &= \frac{1}{2}(Q_{\mathrm{abs},l} + Q_{\mathrm{abs},r}) \\ &= \frac{1}{2}\left(\left\{1 - 2\sum_{p=0}^{N}[E_2^{(p)} + E_4^{(p)}]\right\} \right. \\ &\quad \left. + \left\{1 - 2\sum_{p=0}^{N}[E_3^{(p)} + E_1^{(p)}]\right\}\right) \\ &= 1 - \sum_{p=0}^{N} E^{(p)}, \end{aligned} \tag{30}$$

where

$$\begin{aligned} E^{(p)} &= \sum_{j=1}^{4} E_j^{(p)} \\ &= \sum_{j=1}^{4}\int_0^{\pi/2} |\epsilon_j^{(p)}|^2 \exp\left(-\frac{4\pi m_i}{\lambda} pl\right)\cos\beta d\beta. \end{aligned} \tag{31}$$

The extinction efficiency factor can be obtained as

$$Q_{\mathrm{ext}} = Q_{\mathrm{sca}} + Q_{\mathrm{abs}}. \tag{32}$$

When many cylinders with an oblique incident angle α are randomly located, the intensities from the individual cylinders may be added. Therefore, phase matrix elements G_{kl} for a polydispersion of cylinders are given by the following integration:

$$G_{kl}(m,\alpha,\phi) = \int G_{kl}(x,m,\alpha,\phi)xn(x)dx \Big/ \int xn(x)dx, \qquad k,l = 1,2,3,4, \tag{33}$$

where $n(x)dx$ is the number of particles per unit volume with size parameter between x and $x + dx$. It is noted that if $\mathbf{T}$ is used as the amplitude matrix instead of $\mathbf{A}$, the size distribution $n(x)$ must be substituted instead of $xn(x)$ in Eq. (33).

The method described so far to obtain phase matrix $\mathbf{G}$, adding the complex amplitudes and taking the squared modulus of the combined amplitude, which will be called ray optics A, is exact in the framework of ray optics, but this method still requires a fairly long computation time. On the other hand, if a phase matrix for a polydisperse system is needed, it will be a good approximation to superpose the intensities of the diffracted light and the transmitted light of each order. This alternative method of ray optics will be called ray optics B. For the latter case, the phase matrix elements are expressed as

$$\begin{aligned} G_{kl}(x,m,\alpha,\phi) &= G_{kl}^{D}(x,\alpha,\phi) \\ &\quad + \sum_{p=0}^{N}\sum_{t=1}^{M_p} G_{kl}^{(p)}[x,m,\alpha,\phi(\alpha,\beta_t)], \end{aligned} \qquad k,l = 1,2,3,4, \tag{34}$$

where G_{kl}^{D} and $G_{kl}^{(p)}$ are phase matrix elements generated, respectively, from $(\delta_{1j} + \delta_{2j})A^D$ and $A_j^{(p)}$ by Eq. (23). The elements G_{kl}^{D} can be obtained by $\delta_{kl}|A^D|^2$. In ray optics B, the element G_{12} is taken to be zero at $\phi = 0$ and $\phi = \pi$, similarly to ray optics A. If there is a contribution to the intensity at $\phi = 0$ or π from a ray whose β is not zero, the elements $G_{11}^{(p)}$, $G_{22}^{(p)}$, $G_{43}^{(p)}$, and $G_{44}^{(p)} - G_{12}^{(p)}$ of the corresponding t should be multiplied

by 4.0, since there are two contributions from each side of a cylinder of the same amplitude. The phase factor γ for $A_j^{(p)}$ in Eq. (5) is, in this case, given by $ipl2\pi m_i/\lambda$. Efficiency factors are given in the form

$$\left.\begin{aligned} Q_{\text{ext}} &= 2.0 \\ Q_{\text{sca}} &= \frac{1}{2}(Q_{\text{sca},l} + Q_{\text{sca},r}) \\ &= \frac{1}{2}\left(\left\{1 + 2\sum_{p=0}^{N}[E_2^{(p)} + E_4^{(p)}]\right\}\right. \\ &\quad \left. + \left\{1 + 2\sum_{p=0}^{N}[E_3^{(p)} + E_1^{(p)}]\right\}\right) \\ &= 1 + \sum_{p=0}^{N} E^{(p)} \end{aligned}\right\}. \tag{35}$$

The absorption efficiency factor is obviously given by Eq. (30).

To consider the ground for ray optics B, let us rewrite Eq. (3) as

$$A_j = \sum_{s=0}^{K} a_j^{(s)} \exp[i[\delta_j^{(s)} + \sigma^{(s)}]], \quad j = 1, 2, 3, 4, \tag{36}$$

where $\delta_j^{(s)}$ is the phase factor depending on polarization component j, $\sigma^{(s)}$ is the phase factor common to all polarization components, $a_j^{(s)}$ is the real amplitude of the light ray, K is the number of light rays contributing to the intensity at a direction ϕ. For example, $\delta_j^{(s)}$ = [the phase of $\epsilon_j^{(s)}$], and $\sigma^{(s)} = \gamma$ for the transmitted light of each order; $\delta_j^{(s)} = \sigma^{(s)} = 0$ for the diffracted light. Let us consider the phase matrix element D_{21} in Eq. (24) as an example. Using Eq. (36), D_{21} can be expressed as

$$\begin{aligned} D_{21} = &\sum_{s=0}^{K} a_1^{(s)} a_2^{(s)} \sin[\delta_1^{(s)} - \delta_2^{(s)}] \\ &+ \sum_{\substack{t=0 \\ (t\neq u)}}^{K}\sum_{u=0}^{K} a_1^{(t)} a_2^{(u)} \sin[\delta_1^{(t)} \\ &- \delta_2^{(u)} + \sigma^{(t)} - \sigma^{(u)}]. \end{aligned} \tag{37}$$

If this quantity is integrated over a wide range of size parameters, the double summation of Eq. (37) will be nearly zero, since $\sigma^{(t)} - \sigma^{(u)}$ varies over a wide range. This means that the phase matrix element is composed of superposition of the intensities of the diffracted light and the transmitted light of each order. Moreover, one can easily see that if the scattering body is isotropic and nonabsorbing and no total internal reflection occurs, the element D_{21} becomes nearly zero for a polydisperse system, since $\delta_1^{(s)} - \delta_2^{(s)}$ in Eq. (37) is $\pm\pi$ or zero from the fact that $\delta_j^{(s)}$ = [the phase of $\epsilon_j^{(s)}$] or zero.

IV. Wave Theory

The amplitude matrix elements for wave theory are expressed in such infinite series of the trigonometric functions as

$$T_1(x,m,\alpha,\phi) = a_{02} + 2\sum_{n=1}^{\infty} a_{n2}\cos n\phi, \tag{38}$$

$$T_2(x,m,\alpha,\phi) = b_{01} + 2\sum_{n=1}^{\infty} b_{n1}\cos n\phi, \tag{39}$$

$$T_3(x,m,\alpha,\phi) = 2\sum_{n=1}^{\infty} b_{n2}\sin n\phi, \tag{40}$$

$$T_4(x,m,\alpha,\phi) = 2\sum_{n=1}^{\infty} a_{n1}\sin n\phi. \tag{41}$$

In the above equations, the coefficients a_{n1}, a_{n2}, b_{n1}, and b_{n2} are determined by the boundary condition of continuity of the tangential components of the electromagnetic field at the interface. These coefficients are functions of the Bessel functions of the first kind, the Hankel functions of the second kind, and their first derivatives, whose arguments involve x, m, and α. The detailed expressions for these are found, e.g., in Ref. 7. It is noted here that the relations $b_{n2} = -a_{n1}$ and therefore $T_4 = -T_3$ are always valid and that $T_3 = T_4 = 0$ at $\phi = 0$ and $\phi = \pi$.

The phase matrix is generated from **T** by means of Eq. (23). The efficiency factors for extinction and scattering are given, respectively, by

$$\begin{aligned} Q_{\text{ext}} &= \frac{1}{2}(Q_{\text{ext},l} + Q_{\text{ext},r}) \\ &= \frac{1}{2}\frac{2}{x\cos\alpha}\left\{\left[\text{Re}(b_{01}) + 2\sum_{n=1}^{\infty}\text{Re}(b_{n1})\right]\right. \\ &\quad \left. + \left[\text{Re}(a_{02}) + 2\sum_{n=1}^{\infty}\text{Re}(a_{n2})\right]\right\} \end{aligned} \tag{42}$$

$$\begin{aligned} Q_{\text{sca}} &= \frac{1}{2}(Q_{\text{sca},l} + Q_{\text{sca},r}) \\ &= \frac{1}{2}\frac{2}{x\cos\alpha}\left\{\left[|b_{01}|^2 + 2\sum_{n=1}^{\infty}(|b_{n1}|^2 + |a_{n1}|^2)\right]\right. \\ &\quad \left. + \left[|a_{02}|^2 + 2\sum_{n=1}^{\infty}(|a_{n2}|^2 + |b_{n2}|^2)\right]\right\}. \end{aligned} \tag{43}$$

Namely, we adopted the efficiency factors Q_{ext} and Q_{sca} from the corresponding efficiency factors of Lind and Greenberg[15] divided by $\cos\alpha$. With this definition, Q_{ext} approaches 2.0 with an increase of x for any oblique incident angle α. When the size parameter is small, $Q_{\text{sca},l}$ and $Q_{\text{sca},r}$ are somewhat different from each other (Ref. 5, p. 312). As the size parameter becomes large, the difference between these components decreases for a dielectric cylinder, while for an absorbing cylinder, each component of Q_{sca} is still different from the other even for large size parameters.

V. Numerical Results and Discussion

In geometrical optics, to obtain $\mathbf{A}^{(p)}$ as a function of ϕ it is necessary to solve a $2p$th-order algebraic equation for the pth-order transmitted light, which is the reverse solution of Eq. (17), i.e., $\beta = \beta(\alpha,\phi)$. Computations using geometrical optics were carried out for 181 equally spaced incident directions with angular increments of β of 0.5°. The real amplitude and the phase of $A_j^{(p)}$ for ray optics A and $G_{kl}^{(p)}$ for ray optics B were linearly interpolated at 199 observation angles, 0(0.1)2(1)180°. But except for Fig. 3, figures are drawn at intervals of 2° in ϕ for the sake of comparison with exact wave theory. The computational instability due to the rainbow was removed by the method described in Appendix B. In both cases of ray optics and wave theory, the normalized phase function $G/\overline{Q}_{\text{sca}}$ is drawn in the figures, and, correspondingly, G_{kl}'s generated from amplitude matrix **A** are replaced by $G_{kl}/\overline{Q}_{\text{sca}}$, where

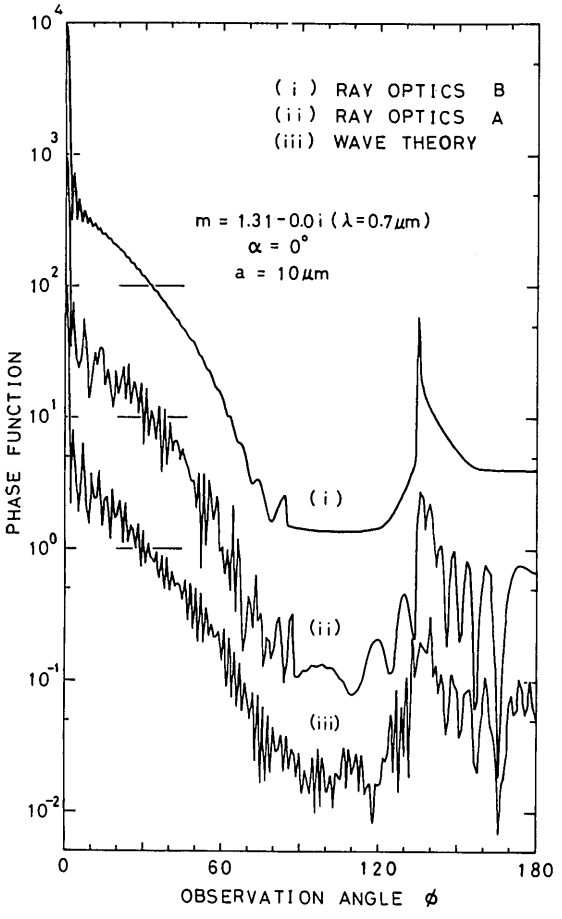

Fig. 3. Phase functions for a single cylinder at normal incidence. The uppermost, middle, and lowermost curves are those computed from ray optics B, ray optics A, and wave theory, respectively. The vertical scale applies to the lowermost curve. The other curves are successively displaced upward by factors of 10, with the horizontal bars occurring where the phase function has the value of unity.

$$\overline{Q}_{sca} = \int Q_{sca} x n(x) dx / \int x n(x) dx. \quad (44)$$

As the complex refractive index of ice, the value of $1.31–0.0i$ at a wavelength of 0.7 μm was adopted.

Figure 3 illustrates the phase functions for a cylinder with 10-μm radius at normal incidence ($\alpha = 0°$). The uppermost curve is that computed from ray optics B by adding the intensities. The steep feature at the very forward direction results from the diffraction. The broad forward lobe results from the transmitted light of the first order, and the primary and secondary rainbows appear concurrently at the observation angle of 135° for $m = 1.31–0.0i$. The middle curve is that computed from ray optics A by adding the complex amplitudes so that the effect of interference is seen overlapping the feature of the uppermost curve. The lowermost curve is that computed from the exact wave theory. Although the frequency of fluctuation due to interference is higher in this case, the overall tendency coincides well with that of the middle curve.

For a large size parameter, since the angular scattering pattern varies rapidly, a comparison should be made with a sufficiently high resolution. However, as the ice crystals in real clouds are not monodispersive but polydispersive, it is reasonable to integrate the contributions over such a size range that the fluctuations due to interference are averaged out. Thus we can accomplish meaningful comparisons with the resolution mentioned above. For the particle size distribution we employed the modified gamma function given by

$$n(x) \propto x^6 \exp(-bx), \quad (45)$$

where b is a constant determined by the average size. Sufficiently wide range was adopted, and the range of integration was divided into sufficiently small intervals in Eq. (33).

Figure 4 compares phase functions at normal incidence for ray optics and wave theory. The average radii are 5, 10, and 30 μm, and corresponding size parameters are 44.9, 89.8, and 269.3, respectively. The phase functions for each size are successively displaced by 1 order of magnitude to allow a clear comparison. We can see that the glory at ϕ (= θ) = 180° that appears for

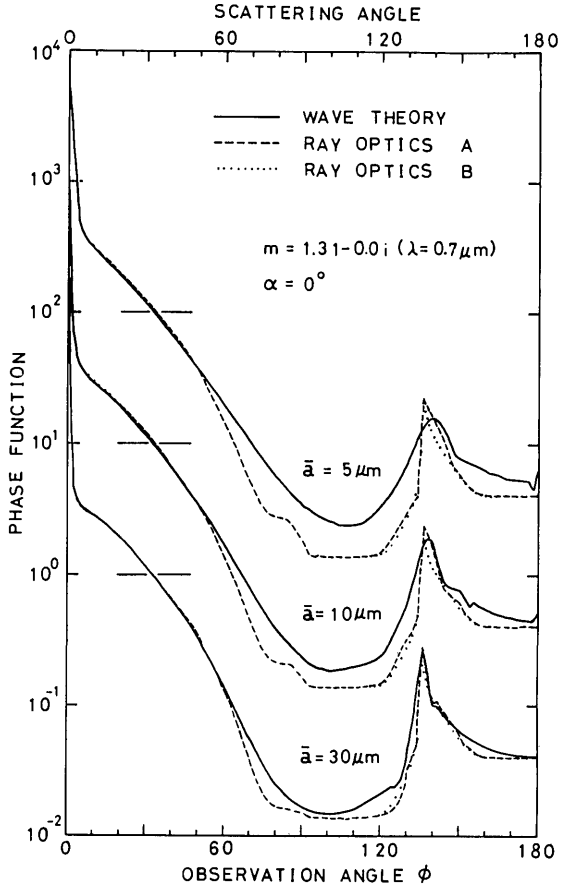

Fig. 4. Comparison of ray optics and wave theory for phase functions at normal incidence. The average radii are 5, 10, and 30 μm. The vertical scale applies to the lowermost curves. The other curves are successively displaced upward by factors of 10. Dotted lines (ray optics B) almost overlap dashed lines (ray optics A) and, moreover, overlap solid lines (wave theory) in the forward direction.

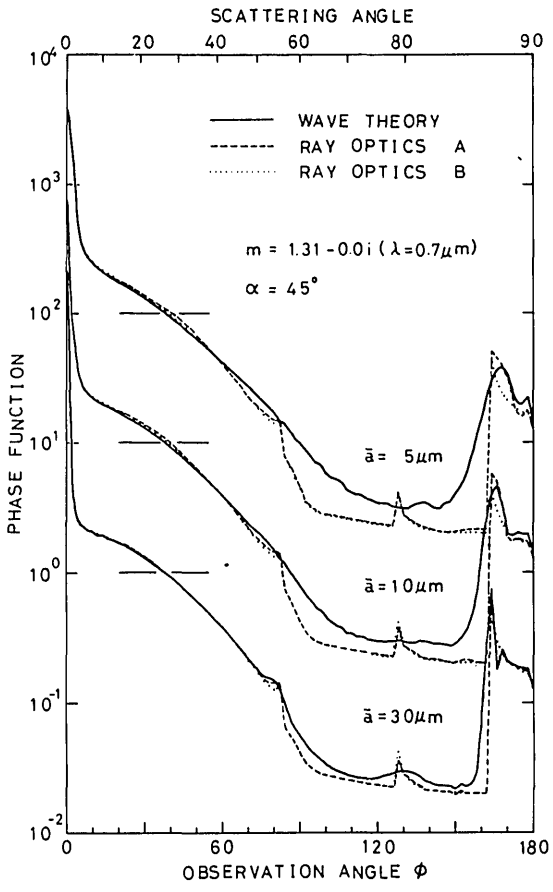

Fig. 5. Same as Fig. 4, but the oblique incident angle α is 45°.

spherical particles[16,17] does not occur in this case and that the normalized intensity of diffracted light at $\phi = 0°$ is proportional to x in this case [Eq. (4)] instead of x^2 for spheres. Some explanations for scattering properties of spherical particles given by Liou and Hansen[16] can be applied to those of cylinders computed by ray optics B and wave theory shown in Fig. 4 and following figures.

In Fig. 5 are compared phase functions obtained by ray optics and wave theory for the oblique incident angles $\alpha = 45°$. The primary rainbow, the secondary rainbow, and the rainbow due to the $p = 5$ component occur, respectively, at observation angles of ~163, 84, and 128°. The rainbow due to the $p = 4$ component at $\phi \simeq 24°$ is not observed clearly because the intense transmitted light of the first order obscures it. The phase function computed by ray optics B does not vary with $\bar{x}$ in the range of backward observation angles ($\phi \geq 90°$) where no diffracted light contributes. This is also the case for other matrix elements produced by ray optics B. On the other hand, as seen from Fig. 5, the phase functions computed by ray optics A vary with $\bar{x}$ ($= 2\pi\bar{a}/\lambda$) even in the range of backward observation angles. Such variations in the case of finite $\bar{x}$ are caused by the effect of interference or the term γ in Eq. (5). It is expected that ray optics B is coincident with ray optics A in the limit of infinitely large $\bar{x}$. Indeed, we can see in the vicinity of the primary rainbow in Fig. 5 that ray optics A and wave theory, which are close to each other, approach ray optics B with an increase of $\bar{x}$

Figure 6 shows comparisons of phase functions by ray optics and wave theory for $\alpha = 85°$. Since calculations by ray optics A were performed at an early stage of this study, only rays up to $p = 9$ were included, but rays up to $p = 12$ were included by ray optics B. Therefore additional rainbows due to components with $p = 10$ and 12 appear at $\phi \simeq 180°$ and $\phi \simeq 170°$, respectively, in ray optics B. For small oblique incident angles α, the phase functions have anisotropic forwardly intense features due to contributions from the diffracted light and the transmitted light of the first order, while for large values of α, especially $\alpha \gtrsim 60°$, they have relatively isotropic features due to the contribution from the externally reflected light.

In Fig. 7, we compare the cross-polarization element G_{12} ($= G_{21}$) computed from wave theory with those computed from ray optics at the oblique incident angles $\alpha = 45°$ and 85°. The curves for $\alpha = 85°$ are displaced upward by factors of 10^2. For $\alpha = 0°$, this element is always zero, because the incident plane is always in the circular cross section of the cylinder. The energy contained within the element G_{12} increases monotonically as the oblique incident angle α increases. As mentioned before, the intensities of the cross-polarization element are zero at $\phi = 0°$ and 180°. For $\alpha = 85°$, we can see a subpeak at $\phi \simeq 4°$ for both wave theory and ray optics B, which is attributable to the rainbow due to the $p = 11$ component. For $\alpha = 45°$, in spite of the discontinuous damping of this element at $\phi = 180°$, the phase

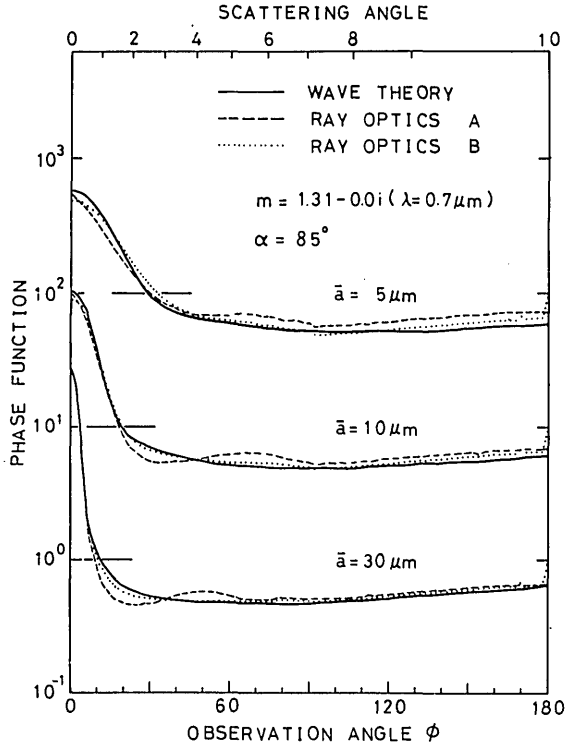

Fig. 6. Same as Fig. 4, but the oblique incident angle α is 85°.

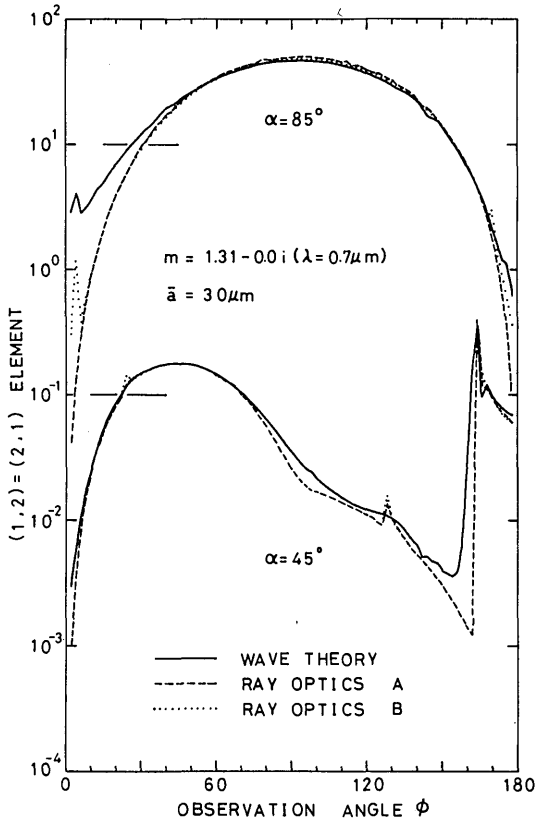

Fig. 7. Comparison of ray optics and wave theory for G_{12}. The average radius is 30 μm. The curves for $\alpha = 85°$ are displaced upward by factors of 10^2, with the horizontal bars occurring where the element has the value 0.1.

functions G have fairly large values at $\phi = 180°$ as shown in Fig. 5. This is attributed to the fact that G_{11} and G_{22} have finite small peaks there and compensate the decrease of the cross-polarization element.

In Fig. 8 the elements G_{11} and G_{22} at the oblique incident angle $\alpha = 85°$ are compared for ray optics and wave theory. The pattern of angular distribution of these elements is nearly symmetrical with respect to $\phi \simeq 90°$ except for the forward observation angle. The large depolarization at $\phi \simeq 90°$ and the symmetrical feature for $\alpha = 85°$ shown in Figs. 7 and 8 result mainly from the way the reference plane for polarization is defined. The reference plane for the incident light is nearly perpendicular to that for the scattered light at $\phi \simeq 90°$ for a large oblique incident angle (see Fig. 1). Therefore, even if the vibrational plane of the electric vector of the light ray hardly varies before and after scattering, a large apparent depolarization is observed around $\phi \simeq 90°$. Using the matrix $\epsilon^{(p)}$ represented before, this apparent large depolarization and symmetrical feature can be explained more concretely as follows. For a large value of α, $\delta 1 \simeq \beta$ from Eqs. (10) and (13), and $r_\parallel$ and $r_\perp$ vary slowly with β, and their values are close to each other. Therefore, from Eq. (6) we have

$$\epsilon^{(0)} \simeq -r_\parallel \begin{pmatrix} \cos\phi & \sin\phi \\ -\sin\phi & \cos\phi \end{pmatrix}.$$

Thus, at the observation angle $\phi \simeq 90°$, the cross-polarization element G_{12} has a maximum value, and the polarization elements G_{11} and G_{22} have minimum values. Moreover, at the observation angle $\phi = 180°$, G_{12} vanishes, and G_{11} and G_{22} have maximum values. Similar considerations can be made for the transmitted rays of higher order.

In Fig. 9 are compared the degree of linear polarization for single scattering of incident unpolarized light at normal incidence, $\alpha = 0°$, by ray optics and wave theory. Although the approximation of ray optics seems to be adequate for small radii such as 10 μm for the scattered intensity (Fig. 4), a much larger average radius of at least 30 μm is necessary to account for the degree of linear polarization with good accuracy.

Figure 10 compares the degree of linear polarization at the oblique incident angles $\alpha = 45$ and 85°. In the case of $\alpha = 45°$, the degree of linear polarization varies suddenly from $\phi = 178°$ to $\phi = 180°$ corresponding to the abrupt change of G_{12} shown in Fig. 7. At $\alpha = 85°$, there is close agreement among ray optics and wave theory. But at $\phi \simeq 180°$, wave theory becomes negatively intense with the increase of $\bar{a}$ compared with ray optics A. This is caused by the rainbow due to the $p = 10$ component, which is clearly seen in ray optics B.

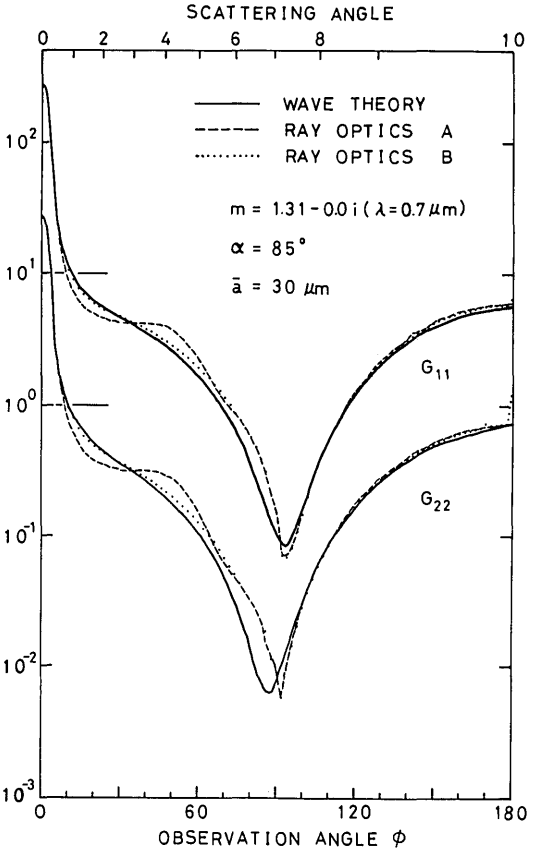

Fig. 8. Comparison of ray optics and wave theory for G_{11} and G_{22} at $\alpha = 85°$. The average radius is 30 μm. The upper curves are displaced upward by factors of 10.

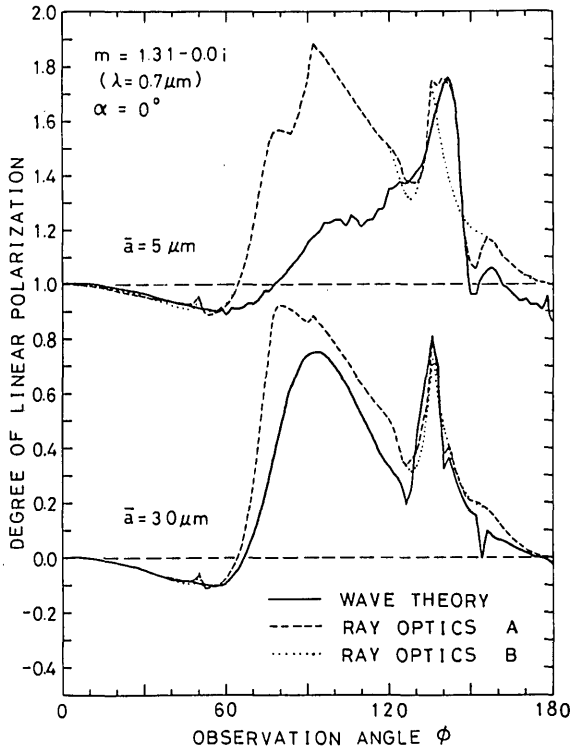

Fig. 9. Comparison of ray optics and wave theory for the degree of linear polarization at normal incidence, $\alpha = 0°$. The average radii are 5 and 30 μm. The zero points of each curve are indicated by the horizontal dashed lines.

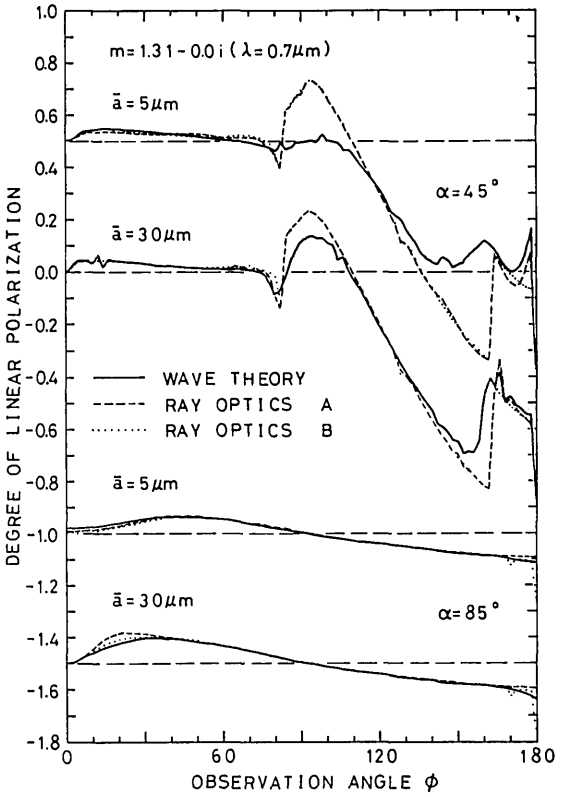

Fig. 10. Same as Fig. 9, but the oblique incident angles α are 45 and 85°.

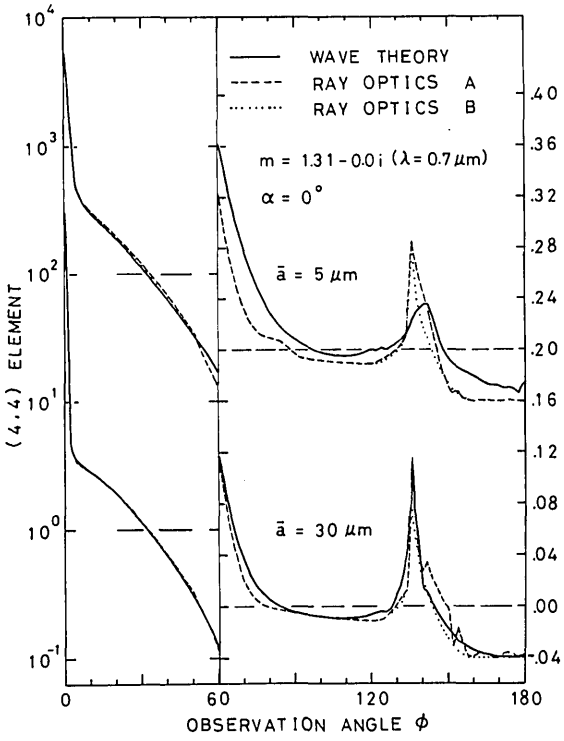

Fig. 11. Comparison of ray optics and wave theory for G_{44} at normal incidence, $\alpha = 0°$. The average radii are 5 and 30 μm. At the observation angle $\phi < 60°$, the left vertical scale applies to the lower curves, and the upper curves are displaced upward by factors of 10^2. At $\phi \geq 60°$, the right vertical scale applies. The zero points of each curve are indicated by the horizontal dashed lines.

The differences at the forward direction among ray optics and wave theory are attributed to the apparent smallness of the cylinders in view of ray optics. From Figs. 9 and 10, it can be thought that the approximation of ray optics for the degree of linear polarization becomes better as the oblique incident angle α increases. At the direction $\phi \simeq 180°$, the degree of linear polarization becomes strongly negative as α increases, but this negative polarization becomes weaker for $\alpha \gtrsim 60°$. This feature is explained as follows. The externally reflected rays at $\phi \simeq 180°$ are those for $\beta \simeq 0°$, $\tau_i \simeq \alpha$, and $\delta 1 \simeq 0°$, so that $\epsilon_2^{(0)} \simeq r_\parallel$ and $\epsilon_1^{(0)} \simeq r_\perp$. The ratio of $|r_\parallel|^2$ to $|r_\perp|^2$ is minimum, when the incident angle α coincides with the Brewster angle, i.e., 52.7° in the case of $m = 1.31\text{–}0.0i$.

Figure 11 shows the G_{44} element at normal incidence, $\alpha = 0°$, for ray optics and wave theory. It is clear that the element G_{44} coincides with the element G_{33}, because $M_3 = 0$ in Eq. (24) at $\alpha = 0°$. The element G_{44} can be approximated by $|A_1| \cdot |A_2|$ at the forward direction, since the amplitudes A_1 and A_2, to which the diffracted light and the transmitted light of the first order contribute, are nearly in phase. Therefore, this element is nearly the same as the phase function $G = (|A_1|^2 + |A_2|^2)/2$, because $|A_1| \simeq |A_2|$ at the forward direction. For $\phi \gtrsim 80°$, the amplitudes of externally reflected rays $A_1^{(0)}$ and $A_2^{(0)}$ become out of phase, because the incident

angle is beyond the Brewster angle, so that G_{44} becomes negative at the direction where the externally reflected light dominates. In the vicinity of the rainbow angle $\phi = 135°$, the amplitudes of the transmitted light of the second order $A_1^{(2)}$ and $A_2^{(2)}$ are in phase, and their values are large, so that G_{44} becomes intensely positive.

Figure 12 shows the element G_{43} ($= -G_{34}$) at normal incidence for ray optics and wave theory. The relative disagreement among them is most conspicuous compared with other phase matrix elements. However, since this element approaches zero over the whole range of observation angles as the average radius increases, the rather remarkable disagreement is not so serious for practical purposes. This tendency becomes more prominent at $\alpha = 45$ and 85°. In this connection, we can add a further comment: in the limit of ray optics (ray optics B), the element G_{43} vanishes regardless of α for a polydisperse system of isotropic dielectric cylinders, while for absorbing cylinders, the element G_{43} by ray optics B does not vanish, and ray optics B is closer to wave theory than ray optics A ($m = 1.31–0.1i$ $\bar{a} = 10\ \mu m$).

Figure 13 compares the efficiency factors for extinction at normal incidence, $\alpha = 0°$, for ray optics and wave theory. There are slowly damping sinusoidal oscillations similar to those for spherical particles. In view of ray optics, an interference of the diffracted light and the transmitted light of the first order is responsible for this oscillatory feature. For Q_{ext} at $\alpha = 45°$, the period of the oscillation in x is shorter, i.e., 10.3 for $\alpha = 0°$ and 7.99 for $\alpha = 45°$, but the patterns are similar to each other.

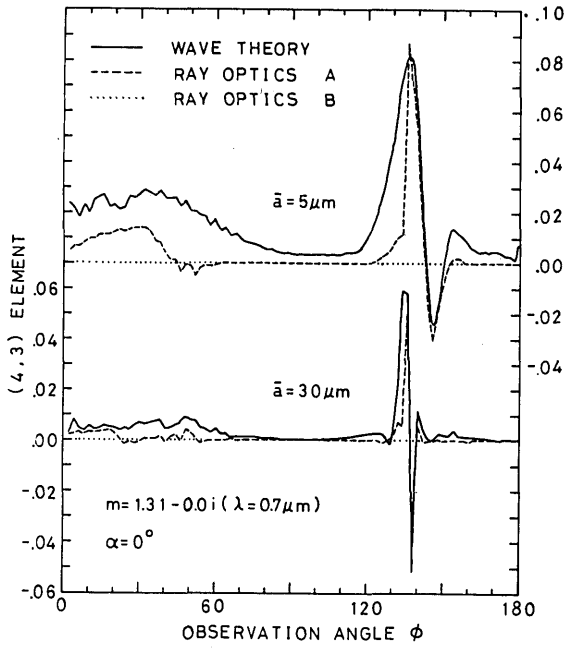

Fig. 12. Comparison of ray optics and wave theory for G_{43} ($= -G_{34}$) at normal incidence, $\alpha = 0°$. The average radii are 5 and 30 μm.

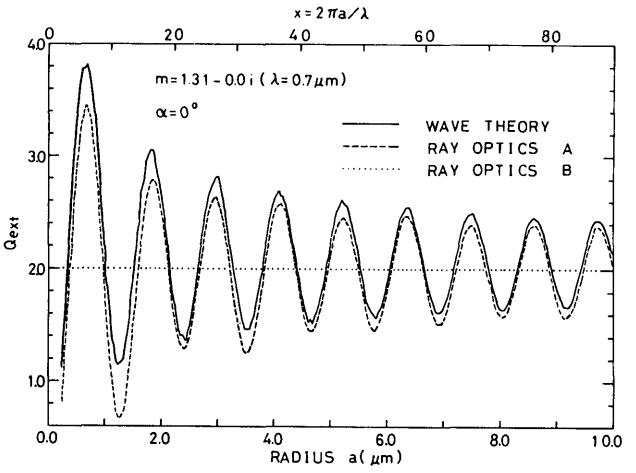

Fig. 13. Comparison of ray optics and wave theory for the extinction efficiency factor Q_{ext} at normal incidence, $\alpha = 0°$.

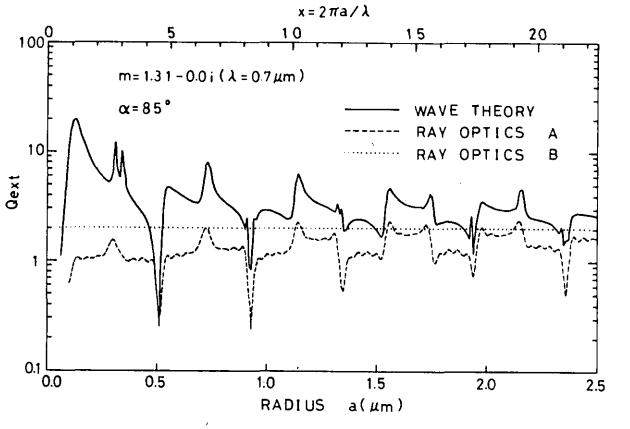

Fig. 14. Same as Fig. 13, but the oblique incident angle α is 85°.

Figure 14 illustrates the extinction efficiency factors at $\alpha = 85°$ for ray optics and wave theory. The variations of Q_{ext} are not sinusoidal in this case but quasi-periodic. The difference between wave theory and ray optics A is larger compared with the case of $\alpha = 0°$, but the positions of the ridges and troughs coincide fairly well with each other. These quasi-periodic variations may be explained in view of ray optics as follows. Because of the large oblique incident angle, the reflectivity is high for internal reflections, so that multiple internal reflection should be considered. Therefore not only the diffracted light and the transmitted light of the first order but also the transmitted light of the higher order interfere with each other, and this interference will generate the quasi-periodic oscillations.

If we include the phase factor $[-2k + (1 - q)/2]\pi/2$ in Eq. (19), there will be a discrepancy on the phase of the oscillation of Q_{ext} between ray optics A and wave theory shown in Figs. 13 and 14. It is noted from Figs. 13 and 14 that the efficiency factor for extinction obtained from wave theory is larger than that obtained

from ray optics A. This difference between wave theory and ray optics A seems to show effects of grazing reflection. But for smaller size parameters, the inapplicability of ray optics is also responsible for the difference in its own right. However, ray optics A will give the extinction efficiency factor more realistically than the anomalous diffraction approximation[5,18] especially in the case of $\alpha = 85°$. Because ray optics A takes into account as many factors as possible, except for the effects of grazing reflection, on the other hand, the anomalous diffraction approximation takes into account only the diffracted light and the transmitted light of the first order for refractive index m close to unity. The behavior of Q_{ext} by wave theory in Figs. 13 and 14, which are equivalent to Figs. 8 or 9 of Ref. 15, is similar to that of slender prolate spheroids (Ref. 19, Fig. 7).

In Table I, the extinction efficiency factors averaged over the size distribution [Eq. (44)] evaluated by ray optics A are compared with those by wave theory. The average extinction efficiency factors are asymptotic to 2.0 from top to bottom in each column.

To examine the effects of absorption, the imaginary part of the complex refractive index was increased by keeping the real part unchanged. Figure 15 shows the phase functions by ray optics and wave theory for the absorbing cylinder with $m = 1.31–0.1i$ ($\lambda = 0.7$ μm). The scattered light intensity consists mainly of the diffracted light and the externally reflected light at any oblique incident angles due to the strong absorption. Therefore, the relative differences among these three methods at the forward direction become more striking, but the absolute differences are nearly the same as those

Table I. Extinction Efficiency Factors Averaged over Size Distribution, Eq. (44), for $m = 1.31–0.0i$ ($\lambda = 0.7$ μm)

	$\alpha = 0°$		$\alpha = 45°$		$\alpha = 85°$	
$\bar{a}$ (μm)	RO(A)	WT	RO(A)	WT	RO(A)	WT
5	1.9659	2.0689	1.9518	2.0981	1.7462	2.3680
10	1.9850	2.0481	1.9706	2.0621	1.8442	2.2511
30	1.9980	2.0127	1.9928	2.0300	1.9261	2.1211

RO(A) = ray optics A; WT = wave theory.

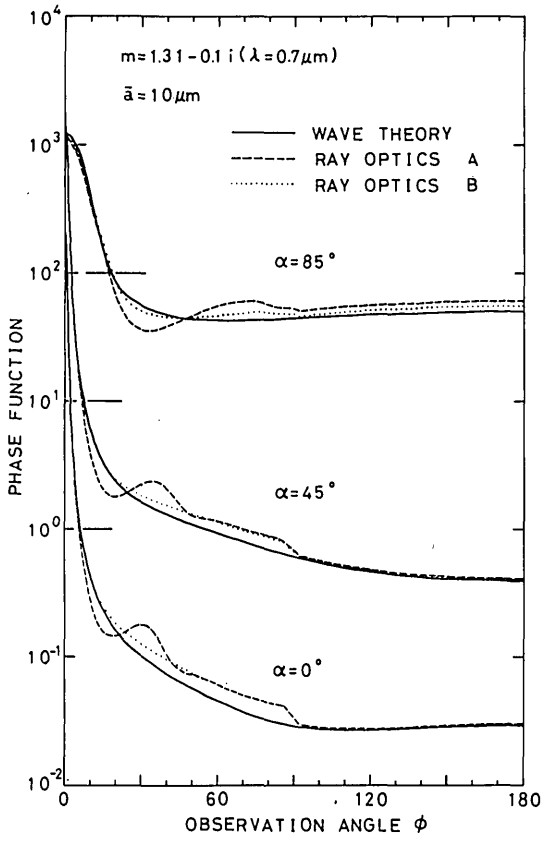

Fig. 15. Comparison of ray optics and wave theory for phase functions at three oblique incident angles for the case of $m = 1.31–0.1i$ ($\lambda = 0.7$ μm). The average radius is 10 μm.

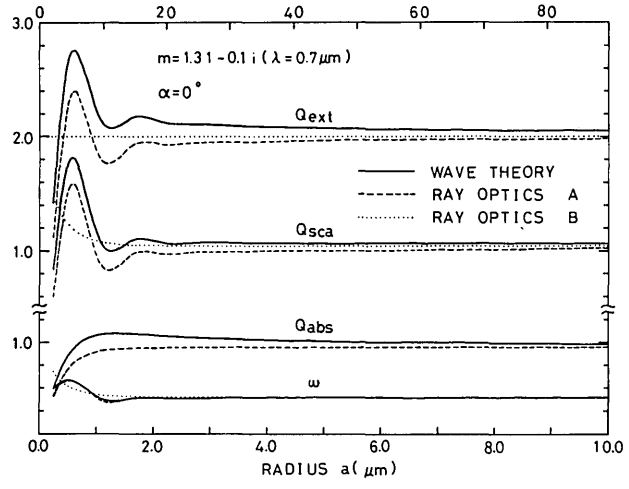

Fig. 16. Comparison of ray optics and wave theory for the efficiency factors for extinction, scattering, and absorption and the single scattering albedo at $\alpha = 0°$ for the case of $m = 1.31–0.1i$ ($\lambda = 0.7$ μm).

for the nonabsorbing case. On the other hand, there is better agreement among ray optics and wave theory at the observation angle $\phi \geq 90°$ for the case of $\alpha = 0$ and 45°.

Figure 16 shows the efficiency factors for extinction, scattering, and absorption, and the single scattering albedo ω for the absorbing cylinder with $m = 1.31–0.1i$ ($\lambda = 0.7$ μm). The efficiency factors for scattering Q_{sca} oscillate for small x, say, $x \leq 30$. As x becomes larger,

Table II. Efficiency Factors for Extinction, Scattering, and Absorption and Single Scattering Albedo Averaged over Size Distribution for $m = 1.31\text{–}0.1i$ ($\lambda = 0.7\ \mu m$) and $\bar{a} = 10\ \mu m$

	$\alpha = 0°$		$\alpha = 45°$		$\alpha = 85°$	
	RO(A)	WT	RO(A)	WT	RO(A)	WT
$\overline{Q}_{ext}$	1.9834	2.0457	1.9704	2.0587	1.8540	2.2465
$\overline{Q}_{sca}$	1.0283	1.0617	1.0453	1.1013	1.5154	1.8602
$\overline{Q}_{abs}$	0.9551	0.9840	0.9251	0.9573	0.3386	0.3863
$\bar{\omega}$	0.5185	0.5190	0.5305	0.5350	0.8174	0.8280

the transmitted light of the first order is almost exhausted, so that the oscillation due to interference disappears. The absorption efficiency factor Q_{abs} computed from ray optics A or B increases monotonically with x and approaches a limiting value, because almost all the light refracted into a large cylinder is absorbed. The radius at which Q_{abs} becomes constant nearly coincides with that at which the oscillation of Q_{sca} disappears. For large sizes, Q_{ext} computed from wave theory and ray optics A approaches 2.0 with slightly decreasing and increasing tendencies, respectively. Although there are some differences in Q_{ext} and Q_{sca} among wave theory and ray optics, the ratio of Q_{sca} to Q_{ext} or the single scattering albedo ω is in good agreement.

Table II gives numerical values of the efficiency factors for extinction, scattering, and absorption, and the single scattering albedo averaged over the size distribution for the absorbing cylinder with $m = 1.31\text{–}0.1i$ ($\lambda = 0.7\ \mu m$), computed by ray optics A and wave theory. The efficiency factors $\overline{Q}_{ext}$ in this case have almost the same values as those of the nonabsorbing cylinders. Ray optics A becomes worse with an increase of α for any efficiency factors. On the other hand, it is fairly good for average single scattering albedo $\bar{\omega}$, which is defined by $\overline{Q}_{sca}/\overline{Q}_{ext}$. The two polarization components of the efficiency factor for extinction $\overline{Q}_{ext,l}$ and $\overline{Q}_{ext,r}$ at $\alpha = 0°$ computed from ray optics A are 1.9826 and 1.9843, and for scattering they are 1.0490 and 1.0077, respectively. On the other hand, those components of the efficiency factor for extinction computed from wave theory are 2.0457 and 2.0456, and for scattering they are 1.0871 and 1.0363, respectively. In the limit of the large size parameter, both polarization components of the extinction efficiency factor should approach 2.0, and each polarization component of the scattering efficiency factor approaches $1 + 2\,[E_2^{(0)} + E_4^{(0)}] = 1.0620$ and $1 + 2\,[E_3^{(0)} + E_1^{(0)}] = 1.0219$, respectively, from Eq. (35).

Figure 17 illustrates the fractions of energy contained in the transmitted light $E^{(p)}(x,m,\alpha)$ of the different order p as a function of the oblique incident angle α for the case of $m = 1.31\text{–}0.0i$ ($\lambda = 0.7\ \mu m$). The main feature of $E^{(p)}$ can be explained schematically as follows. Let us consider a ray of light incident on a cylinder toward the central axis of the cylinder and denote Fresnel reflection energy $|r_\parallel|^2$ or $|r_\perp|^2$ as r for the sake of simplicity. Then the energy of externally reflected light and the energy of transmitted light of the first order are expressed as r and $(1 - r)^2$, respectively.

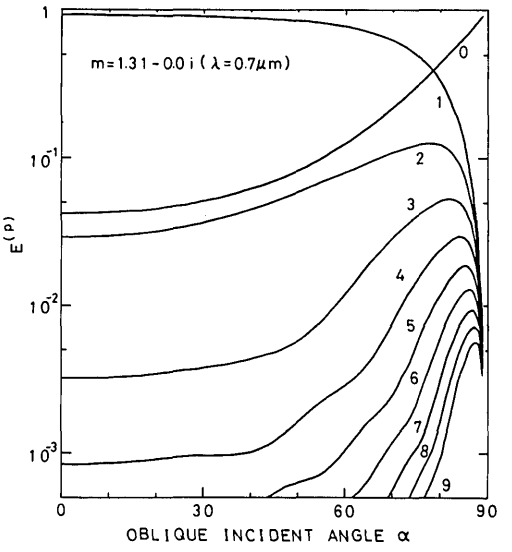

Fig. 17. Fractions of energy contained in the transmitted light $E^{(p)}(x,m,\alpha)$ of the different order p for $m = 1.31\text{–}0.0i$ ($\lambda = 0.7\ \mu m$). The numbers in the figure denote p.

Therefore $E^{(0)}$ increases and $E^{(1)}$ decreases monotonically with α due to the increase of r. The energy of transmitted light of the pth order ($p \geq 2$) is generally expressed by the geometrical series

$$r^{p-1}(1 - r)^2, \tag{46}$$

where the common ratio is $r(\leq 1)$. When α is relatively small where r is also small, the increase of reflection term r^{p-1} in Eq. (46) with a small increase of r overcomes the decrease of transmission term $(1 - r)^2$, so that the energies contained in the transmitted light of the higher order increase. On the other hand, when α becomes large where r increases rapidly, the decrease of transmission term overcomes the increase of reflection term, so that $E^{(p)}$ ($p \geq 2$) decreases, and the convergence of the series becomes slow and a large number of terms is required. For a ray of light incident on any position of a cylinder, the situation is the same as the above. Variations of $E_1^{(p)}$, $E_2^{(p)}$, and $E_3^{(p)}$ for $p \geq 2$ with α are not so simple as $E^{(p)}$ but rather winding. $E_1^{(p)}$ and $E_2^{(p)}$ increases where $E_3^{(p)}$ decreases and vice versa. This means that by a rotation of the incident plane, the radiant energy is distributed among the different polarization components, but $E^{(p)}$, which is the average of these components, varies fairly simply as shown in Fig. 17.

VI. Conclusions

After the above comparison of ray optics and the exact electromagnetic wave theory for several quantities for single scattering by circular cylinders, it has become evident that the applicability of the approximation of ray optics is dependent on the orientation of cylinders relative to the incident light as well as their size parameters. The applicability of ray optics also depends on what quantity for single scattering (e.g., the phase function, the degree of linear polarization, the extinction efficiency factor, or the single scattering albedo) is compared. Although in this study we investigated applicability of ray optics for the size parameters up to $\simeq 270$, much larger size parameters of the order of several hundreds seem to be needed for valid application of the ray optics approximation to all the single scattering quantities. The variations of phase matrix elements and scattering cross sections with the size parameter computed by ray optics A agreed with those by wave theory, but the method of ray optics A still requires a fairly long computation time. On the other hand, the approximation of ray optics B gives fairly accurate phase matrix elements for a polydisperse system, and a much less computer time is needed. For example, for $m = 1.31\text{–}0.0i$ ($\lambda = 0.7\ \mu$m) and $\bar{a} = 30\ \mu$m the computation time by ray optics B is only $0.4 \sim 4\%$ of the corresponding time by wave theory, whereas ray optics A requires about 20–160% of wave theory. From an optical point of view, it may be useful to study further the solution of ray optics A, but from a point of practical use, e.g., in meteorology, ray optics B will provide a convenient means to investigate the phase matrix of other nonsperical particles like hexagonal cylinders.

The authors wish to express their hearty thanks to S. Asano for his critical reading of the manuscript and for discussions. This study was supported by Scientific Research Funds from the Ministry of Education of Japan. The numerical computations were made on the ACOS700 computer at Tohoku University.

Appendix A

Applying Huygens's principle and Babinet's theorem (Ref. 5, p. 105), the disturbance u_s caused by diffraction about a circular cylinder is expressed as

$$u_s = -\frac{i}{R\lambda} u_i \int_{-\infty}^{\infty} \int_{-a}^{a} \exp\left\{ i \left[\omega t - k(X\cos\alpha + Z\sin\alpha) - k\bar{r} \right] \right\} dY dZ. \tag{A1}$$

Here u_i is the disturbance in the original wave, the term $\omega t - k\,(X\cos\alpha + Z\sin\alpha)$ denotes the phase of the plane wave incident on the infinitely long slit at an oblique incident angle α, and $\bar{r}$ is the distance from a point $(0,Y,Z)$ in the slit to an observation point with sufficiently large R; i.e.,

$$\bar{r} = R\left(1 - \frac{2Y}{R}\cos\alpha\sin\phi - \frac{2Z}{R}\sin\alpha + \frac{Y^2+Z^2}{R^2}\right)^{1/2}$$

$$\simeq R - Y\cos\alpha\sin\phi - Z\sin\alpha + \frac{Z^2}{2R}. \tag{A2}$$

Thus, the explicit expression for the amplitude can be obtained by direct integration of Eq. (A1) as

$$\mathbf{E}_s = (2x\cos\alpha)^{1/2} \frac{\sin(x\cos\alpha\sin\phi)}{x\cos\alpha\sin\phi} \left(\frac{x}{\pi kR}\right)^{1/2} \times \exp\left[i\left(\omega t - kR - \frac{3}{4}\pi \right) \right] \mathbf{E}_i. \tag{A3}$$

Here the disturbances u_i and u_s are interpreted, respectively, as $(\cos\alpha)^{1/2}\mathbf{E}_i$ and $\mathbf{E}_s$. Comparing Eq. (A3) with the definition of the amplitude matrix, we easily find that A_D is given by Eq. (4).

Appendix B

When a rainbow appears, the fraction of energy contained in the transmitted light of the order responsible for the rainbow is obtained by integrating the intensity over the observation angle; i.e.,

$$\omega_j^{(p)} = \frac{1}{\pi} \int_0^{\pi} |A_j^{(p)}|^2 d\phi, \quad j = 1, 2, 3, 4. \tag{B1}$$

The energy thus determined does not always agree with the fraction of energy contained originally in the transmitted light of that order $E_j^{(p)}$ because $\omega_j^{(p)}$ involves instability resulting from the fact that $A_j^{(p)}$ has an infinite value at an exact rainbow angle. The classical theory of geometrical optics fails also in the vicinity of the rainbow angle. Therefore, we intend to remove the instability of $\omega_j^{(p)}$ or Q_{sca} and to correct the intensity at an approximate rainbow angle ϕ_R by replacing $A_j^{(p)}$ at ϕ_R with

$$\begin{matrix} \eta_j^{(p)} \exp\{i \arg [A_j^{(p)}]\}, & \text{for } [\eta_j^{(p)}]^2 \geq 0 \\ 0, & \text{for } [\eta_j^{(p)}]^2 < 0 \end{matrix}, \tag{B2}$$

where

$$\eta_j^{(p)} = \{|A_j^{(p)}|^2 - [\omega_j^{(p)} - E_j^{(p)}]/\Delta w\}^{1/2}, \tag{B3}$$

and Δw is the quadrature weight at ϕ_R. The sign of the factor $[\eta_j^{(p)}]^2$ was often found to be negative for small x, but it became almost positive for large x.

References

1. H. K. Weickmann, Ber. Dtsch. Wetterdienstes **6**, 54 (1949).
2. A. Heymsfield, J. Atmos. Sci. **32**, 799 (1975).
3. Lord Rayleigh, Philos. Mag. **36**, 365 (1918).
4. J. R. Wait, Can. J. Phys. **33**, 189 (1955).
5. H. C. van de Hulst, *Light Scattering by Small Particles* (Wiley, New York, 1957).
6. M. Kerker, D. D. Cooke, W. A. Farone, and R. T. Jacobsen, J. Opt. Soc. Am. **56**, 487 (1966).
7. K.-N. Liou, Appl. Opt. **11**, 667 (1972).
8. D. Marcuse and H. M. Presby, J. Opt. Soc. Am. **65**, 367 (1975).
9. R. D. Birkhoff, J. C. Ashley, H. H. Hubbell, Jr., and L. C. Emerson, J. Opt. Soc. Am. **67**, 564 (1977).
10. T. B. A. Senior and H. Weil, Appl. Opt. **16**, 2979 (1977).
11. H. M. Presby, J. Opt. Soc. Am. **64**, 280 (1974).
12. D. Marcuse, Appl. Opt. **14**, 1528 (1975).
13. J. Holoubek, Appl. Opt. **15**, 2751 (1976).
14. C. Saekeang and P. L. Chu, J. Opt. Soc. Am. **68**, 1298 (1978).
15. A. C. Lind and J. M. Greenberg, J. Appl. Phys. **37**, 3195 (1966).
16. K.-N. Liou and J. E. Hansen, J. Atmos. Sci. **28**, 995 (1971).
17. K.-N. Liou, J. Atmos. Sci. **29**, 524 (1972).
18. D. A. Cross and P. Latimer, J. Opt. Soc. Am. **60**, 904 (1970).
19. S. Asano, Appl. Opt. **18**, 712 (1979).